CYCLE-BY-CYCLE SIMULATION OF VARIABLE AMPLITUDE FATIGUE CRACK PROPAGATION

L. Muys[1], J. Zhang[2,3], N. Micone[3], W. De Waele[3] and S. Hertelé[3]

[1] Ghent University, Belgium
[2] SIM vzw, Technologiepark 935, BE-9052 Zwijnaarde, Belgium
[3] Ghent University, Laboratory Soete, Belgium

Abstract: In variable amplitude fatigue of high strength low alloy (HSLA) steel components, overloads can severely retard subsequent crack propagation for a number of cycles. In order to be able to predict fatigue crack propagation with a reduced degree of conservatism, retardation has to be taken into account. Of all numerical models that have been developed over time, crack tip plasticity models are selected based on the need for a detailed and fast cycle-by-cycle simulation of high cycle. After introducing the load interaction zone concept, common to all crack tip plasticity models, the Wheeler and Willenborg models are discussed, implemented and compared to experimental data. It is concluded that the Modified Wheeler model provides the most promising results, whereas the main limitation of Willenborg models is the need for extensive experimental data.

Keywords: fatigue; variable amplitude; retardation; crack tip plasticity models; wheeler; willenborg

NOMENCLATURE

a	crack length	m
a_{OL}	overload crack length	m
ΔK	stress intensity factor range	$\mathrm{MPa}\sqrt{\mathrm{m}}$
ΔK_{th}	threshold stress intensity factor range	$\mathrm{MPa}\sqrt{\mathrm{m}}$
$K^*_{\max}$	'no retardation' stress intensity factor	$\mathrm{MPa}\sqrt{\mathrm{m}}$
r_{p}	plastic zone size	m
$r_{\mathrm{p,OL}}$	overload plastic zone size	m
r^*_{p}	'no retardation' plastic zone size	m
R_{SO}	shut-off overload ratio	-
β	plastic zone size factor	-
σ_y	yield strength	MPa

1 INTRODUCTION

The effects of variable amplitude loading on fatigue crack propagation were first observed by the airplane industry. It was found that linear cumulative damage evolution (as predicted with Miner's rule) was often ultra-conservative. Experiments revealed that after applying a single overload cycle in between constant amplitude loading cycles, crack propagation was slower than for constant amplitude fatigue [1]. This effect was called *retardation*. In an attempt to lower the degree of conservatism of a fatigue design – and thus indirectly the safety factor, material usage and cost – researchers tried to account for the retardation effect. Most studies have focused on the behavior of aluminum alloys, which were frequently used in that industry at the time [1–5].

Lately, there has been a lot of interest in the offshore industry for simulating variable amplitude fatigue crack propagation [6,7]. Offshore constructions are continuously subjected to variable loading conditions, due to various influences from sea and wind current amongst others. As this problem concerns high cycle fatigue, a first requirement for a suitable cycle-by-cycle fatigue crack propagation model is a reasonable total computation time. Additionally, the model should be able to yield satisfactory results without requiring extensive experimental material characterization. As most models have been developed for aluminum, good correlation for offshore steel grades is not guaranteed.

The ambition of this work is to study the influence of single overload cycles or a sequence of overloads, and thus to analyze a complete load history cycle by cycle. Over time, numerous methods have emerged, but most can be classified in one of 2 main categories: crack tip plasticity models and crack closure models. In general, crack closure models require extensive experimental characterization and/or numerical calculations, and thus do not meet the requirements stated above. Crack tip plasticity models however are better suited. These models are reviewed in detail in Section 2 and their implementation into an algorithm is explained in Section 3.

The behavior and correlation of the chosen models is demonstrated and discussed in Section 4. Input is taken from the work of De Tender [7,8], who performed variable amplitude block loading tests on offshore steels. The definition of the block loading schemes was based on an extensive analysis of wave spectra acting on a monopile structure. These were translated into a series of ΔK-blocks applied to eccentrically loaded side edge tensile (ESET) specimens.

2 CRACK TIP PLASTICITY MODELS

Crack tip plasticity models account for variable amplitude effects by considering the state of the material in front of the crack tip, where some regions have undergone yielding while others have not. To this purpose, the plastic zone induced at the crack tip is discussed first. Based on this, the load interaction zone concept, common to all crack tip plasticity models, is introduced and illustrated with two prominent models, the Wheeler model and the Willenborg model.

2.1 Plastic zone

Linear elastic stress analysis of sharp cracks predicts infinite stresses at the crack tip. In reality however, the stresses are finite due to a finite crack tip radius and plastic deformation in front of the crack tip [9]. The general formula for calculating the plastic zone size is given by Eq. (1).

$$r_{\mathrm{p}} = \frac{1}{\beta\pi}\left(\frac{K}{\sigma_y}\right)^2 \tag{1}$$

Two main methods for calculating the size of the plastic zone are proposed in literature [9]: Irwin's approach and the strip-yield model. According to Irwin, the plastic zone size factor β has a value of 1.0 for plane stress. For plane strain, the value is 3.0, due to suppression of yielding by the triaxial stress state. The strip-yield model predicts a value of 0.81 for plane stress, resulting in a slightly larger plastic zone as opposed to Irwin's result. For plane strain the predicted value of 5.07 deviates significantly from Irwin's calculations [10]. As neither plane stress nor plane strain are real-life scenarios, relations have been developed to include the influence of applied load and specimen thickness [11]. Willenborg [2] originally used Irwin's pane stress result while Wheeler [1] employed a plane strain value of $2\sqrt{2} \approx 2.8$, also deduced from Irwin's work.

2.2 Load interaction zone concept

The state of the material in front of the crack tip considered by crack tip plasticity models is illustrated in Figure 1. It contains the locations of all relevant elastic-plastic yield interfaces caused by current or previous fatigue cycles, and is therefore a representation of relevant loading history. In case of a single overload occurring at crack length a_{OL}, the material yields in the vicinity of the crack tip and a plastic zone of size $r_{\mathrm{p,OL}}$ is caused. Subsequent nominal loads, applied at increasing crack length a, will cause plastic zones of size r_{p} in front of the propagating crack tip. Since $r_{\mathrm{p}} < r_{\mathrm{p,OL}}$, the current plastic zone will be fully embedded in the overload plastic zone for a certain number of cycles. It is assumed that crack growth rate is reduced during these cycles. Once the current elastic-plastic interface intersects the one caused by the overload, the current plastic zone becomes the relevant plastic zone and the interaction effect disappears. Based on this reasoning, the condition for retardation becomes $r_{\mathrm{p}}^* > r_{\mathrm{p}}$ [1]. r_{p}^* represents the hypothetical size that the current plastic zone should have in order for it to touch the overload elastic-plastic interface.

As the crack propagates, r_{p}^* approaches r_{p}, and the retardation effect weakens. Willenborg [2] proposed to quantify the retardation effect by using a combination of both values, since their difference represents the proximity of both elastic-plastic interfaces. Later, the hypothetical stress intensity factor K_{max}^*, Eq. (2), corresponding to r_{p}^* was introduced [3] by assuming a constant plastic zone size factor. Evidently, load interaction occurs when the 'no retardation' stress intensity factor (SIF) K_{max}^* exceeds K_{max}.

$$K_{\mathrm{max}}^* = K_{\mathrm{max,OL}}\sqrt{1 - \frac{a - a_{\mathrm{OL}}}{r_{\mathrm{p,OL}}}} \tag{2}$$

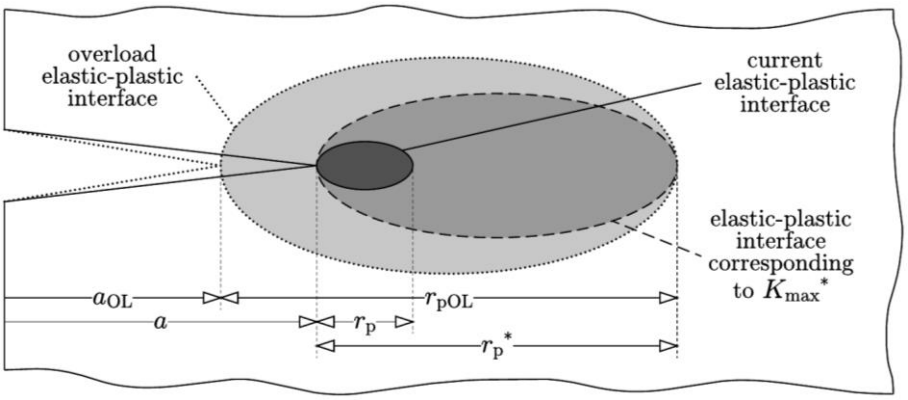

Figure 1: Post-overload plastic zones considered in crack tip plasticity models

Although the Wheeler model, Section 2.3, and the Willenborg model, Section 2.4, are based on the same load interaction zone concept, they differ in two ways: the stress intensity factors $K_{\max}^*$ and $K_{\max}$ are differently combined and the influence on the net crack growth rate is either direct or undirect, respectively. In the following sections, the model equations will be stated in terms of $K_{\max}^*$ for the sake of simplicity. However, in case the assumption of a constant plastic zone shape factor is not acceptable, the model equations have to be expressed in terms of r_{p}^*.

2.3 Wheeler

Wheeler [1] observed that fatigue lifetime predictions based on linear cumulative crack growth (as calculated with Miner's rule) were often found to be ultra-conservative. Therefore, he modified Miner's rule by introducing a retardation factor ϕ_{wh}, which takes a positive value below 1, with 1 being the case of no interaction. The Wheeler model does not alter input for the crack growth law (e.g. ΔK and R), so the straightforward Paris equation can be employed, provided that it was obtained under the correct load ratio. This is illustrated in Eq. (3), in which n is the number of applied cycles and ΔK_i is the SIF range of cycle i. Load interaction effects can potentially be simulated as the net crack growth rate is no longer independent of prior load history.

$$a_n = a_0 + \sum_{i=1}^{n} \phi_{wh,i}\, C(\Delta K_i)^m \tag{3}$$

The retardation factor, given in Eq. (4), is obtained by combining $K_{\max}^*$ and $K_{\max}$ as a ratio and raising it to the power $2w$. Originally, the shaping exponent w had to be determined experimentally for a given material and type of loading, as dependence on these factors was observed [1,12,13]. Typical reported values range from 1.0 up to 4.0. The factor 2 in the exponent is due to historical reasons. As $\phi_{wh} = 0$ is not possible (unless $K_{\max} = 0$), the Wheeler model will never predict crack arrest. This is a major difference to the Willenborg model.

$$\phi_{wh} = \begin{cases} \left(\frac{K_{\max}}{K_{\max}^*}\right)^{2w}, & K_{\max}^* > K_{\max} \\ 1, & K_{\max}^* \leq K_{\max} \end{cases} \tag{4}$$

The experimental parameter w was, besides being impractical, not applicable in general. Therefore, a theoretical relation, Eq. (5), was proposed [5,14]. It is based on the observation of crack arrest for overload values above a specific load ratio value R_{SO}, typically ranging from 1.5 to 3.0, depending on the material. It was reasoned that at the onset of crack arrest, the effective SIF range must not exceed the threshold SIF range for the material. As m is the Paris exponent, the shaping exponent can be determined from readily available material data. It is no longer a constant but a function of the material and the subsequent loading cycles.

$$w = \frac{m}{2}\left(\log\frac{\Delta K_{th}}{\Delta K} \Big/ \log\frac{1}{R_{SO}}\right) \tag{5}$$

2.4 Willenborg

Willenborg [2] assumed that retardation occurs because the stresses caused by the current load cycle are reduced due to residual compressive stresses within the overload plastic zone. This reduction was redefined in terms of a reduction in stress intensity factor [4]. Whereas Wheeler defined a ratio, Willenborg quantifies K_{red} through subtraction, without the use of an experimental parameter. The effective SIF range and load ratio are calculated by reducing both $K_{\max}$ and $K_{\min}$ by K_{red} and requiring them to be non-negative. The governing equations are given by Eqs. (6-8).

$$K_{\mathrm{red}} = K_{\max}^* - K_{\max} \tag{6}$$

$$R_{eff} = \begin{cases} \frac{K_{\min} - K_{\text{red}}}{K_{\max} - K_{\text{red}}}, & K_{\text{red}} < K_{\min} \\ 0, \; K_{\min} \leq K_{\text{red}} < K_{\max} \end{cases} \tag{7}$$

$$\Delta K_{eff} = \begin{cases} \Delta K, & K_{\text{red}} < K_{\min} \\ K_{\max} - K_{\text{red}}, \; K_{\min} \leq K_{\text{red}} < K_{\max} \end{cases} \tag{8}$$

Crack arrest happens for high overload ratios, leading to high residual stress in the overload plastic zone and $K_{\text{red}} \geq K_{\max}$. For small overload ratios ($K_{\text{red}} < K_{\min}$) only the load ratio R is modified and a crack growth law dependent on both ΔK and R is required [3].

A deeper study of Eqs. (6-8) shows that crack arrest is predicted for an overload ratio of 2 at all times. However, literature indicates that the overload value at crack arrest is variable, as discussed in Section 2.3. This can lead to unconservative predictions [4]. In reality, crack arrest happens at both a characteristic threshold SIF range and a characteristic overload ratio. To accommodate for this, a correction factor λ for K_{red} is introduced, given by Eq. (9). If this correction is used, the model is called the Generalized Willenborg Model [15]. The use of the Paris equation combined with Willenborg models was found to be a decent option in cases where the load ratio effect cannot be quantified [4].

$$\lambda = \frac{1 - \frac{\Delta K_{th}}{\Delta K}}{R_{SO} - 1} \tag{9}$$

3 CYCLE-BY-CYCLE ALGORITHM

As previously stated, crack tip plasticity models analyze each applied cycle individually. Therefore, an algorithm was developed in Python to be able to process a large amount of cycles in an automated way. A schematic overview of this algorithm is given in Figure 2.

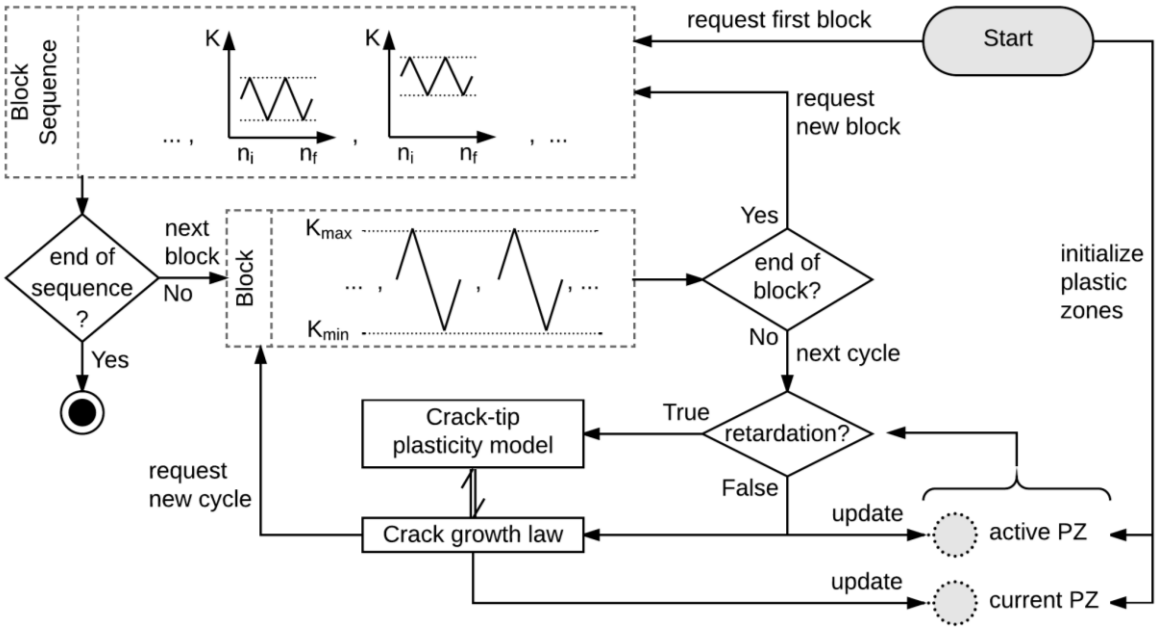

Figure 2: Schematic overview of cycle-by-cycle algorithm

Before the analysis is started, the input load history is translated into a block sequence. It is basically a series of blocks in which every block contains the maximum and minimum applied SIF of the block-specific fatigue cycle and the number of experimentally applied cycles. Once the analysis is started, the state of the load interaction zone has to be initialized. The active plastic zone is the largest plastic zone (PZ), possibly caused by an earlier overload cycle, while the current plastic zone is formed by the latest cycle. The input needed for initializing both plastic zones is derived from a fatigue pre-cracking history. It can be safely assumed that at the end of this procedure no load interaction effects were in play, meaning that both plastic zones are equal and can be defined by the initial crack length and the maximum SIF applied during pre-cracking.

After initialization, the first cycle of the first load block is loaded and analyzed. First the sizes of the current and active plastic zones are compared to decide whether load interaction occurs. After pre-cracking this is not the case, so the active PZ is updated to the current plastic zone. The crack growth law calculates the increment based on the unaltered SIF values and updates the current PZ based on the calculated increment. Further in the load spectrum, an overload can be applied. If the condition for retardation is true, the unmodified

SIF values are sent to the crack tip plasticity model, which will alter the input for – or output from – the crack growth law. The modified increment is then used to update the current PZ. Note that the active PZ is not updated since load interaction is occurring.

4 ANALYSIS RESULTS

This section compares crack growth predictions using different crack tip plasticity based retardation models against experimental data.

In the previous sections, disagreement between employed plastic zone shape factors was brought to attention. In order to compare both crack tip plasticity models objectively, a common β-factor has to be employed. This factor is dependent on both the applied load and specimen thickness, and a condition for plane strain was introduced [11]. Based on this condition, the thickness of our specimen is well above the required thickness for plane strain, even for the maximum applied load. A value of $\beta = 2\sqrt{2}$ will be used throughout this analysis.

The applied load history, a low-high-low sequence [16] is visualized in the upper part of Figure 3. The ΔK-values have been plotted with respect to the cumulative number of cycles. All loads were applied with $R = 0.1$. For the material used, the Paris law constants are available for this specific load ratio only. The influence of this limitation will be discussed further. During the first 5 blocks, no interaction effect is predicted as the load is increased for every block. For these blocks, all simulations correlate well with measured crack growth, as can be observed in the bottom part of Figure 3. For the last 4 blocks, retardation manifests and the shortcomings of linear cumulative crack growth (illustrated by the dashed line) become clear. For the purpose of visibility, graphs further in this analysis will only show the last 4 blocks.

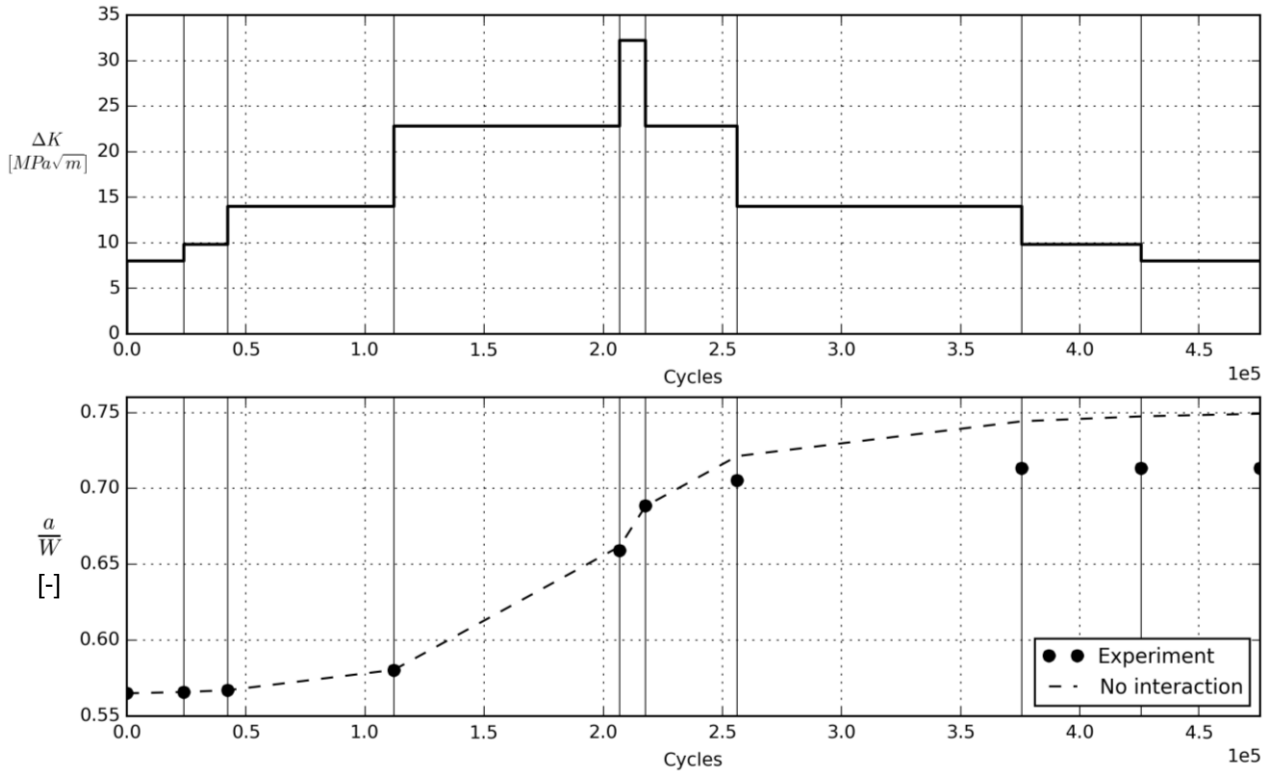

Figure 3: Input loading history (top) and experimental and predicted crack growth (bottom)

The importance of the shut-off overload ratio R_{SO} (for which crack arrest happens) has been discussed higher. For the material under investigation, a dependency on the applied load has been observed. For low SIF ranges, crack arrest even occurred for values below 2. Due to the small number of observations, only an upper bound for $R_{SO}(\Delta K)$ could be established. Therefore, the simulated Modified Wheeler and Generalized Willenborg models provide an upper bound on the predicted crack growth. Improvement of the results is likely if $R_{SO}(\Delta K)$ could be obtained in more detail.

In order to gauge the improvement that the crack tip plasticity models provide, the predictions have to be compared to the linear cumulative crack growth curve, which provides an upper bound. This upper bound is drawn as a dashed line in Figure 4 and Figure 5. The real crack growth was only measured in between loading blocks and is represented by the dotted line. Crack arrest can be noticed after the second block. Ideally, the employed models should predict such crack arrest.

The results of a comparison of the different Wheeler models are shown in Figure 4. For the original model, $w = 3.4$ was found to give the best fit with the experiment. Retardation is underestimated in the first block and overestimated elsewhere. A potential cause is the constant shaping exponent, which does not account for load and proximity to crack arrest. This inconsistency is resolved in the modified Wheeler model, which systematically underestimates the retardation effect. While the original model seems to provide better agreement, it has to be noted that it is the result of arbitrary fitting without much scientific foundation. The modified Wheeler model on the other hand is analytically derived and its earliest results are satisfactory, taking into account that it is merely an upper bound. Both models incorrectly predict crack propagation (instead of crack arrest) after the second block. This is an implication of the direct approach, i.e. correcting the normal non-zero crack growth rate by a non-zero factor, instead of altering the input for the crack growth law.

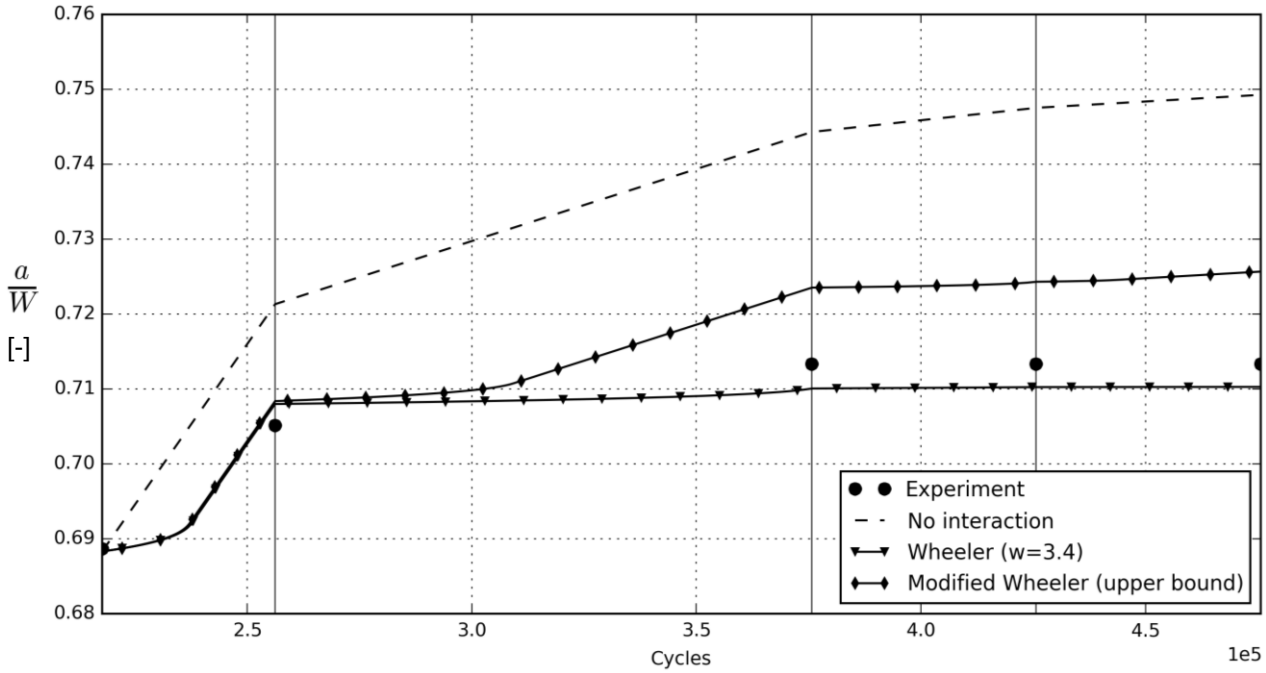

Figure 4: Comparison of the Wheeler and Modified Wheeler model

Both Willenborg models have been analytically established and do not require a fitting parameter, so they can be compared objectively. The original Willenborg model severely underestimates the retardation effect. A potential and most obvious reason is the fact that the influence of the effective load ratio R_{eff} is ignored by

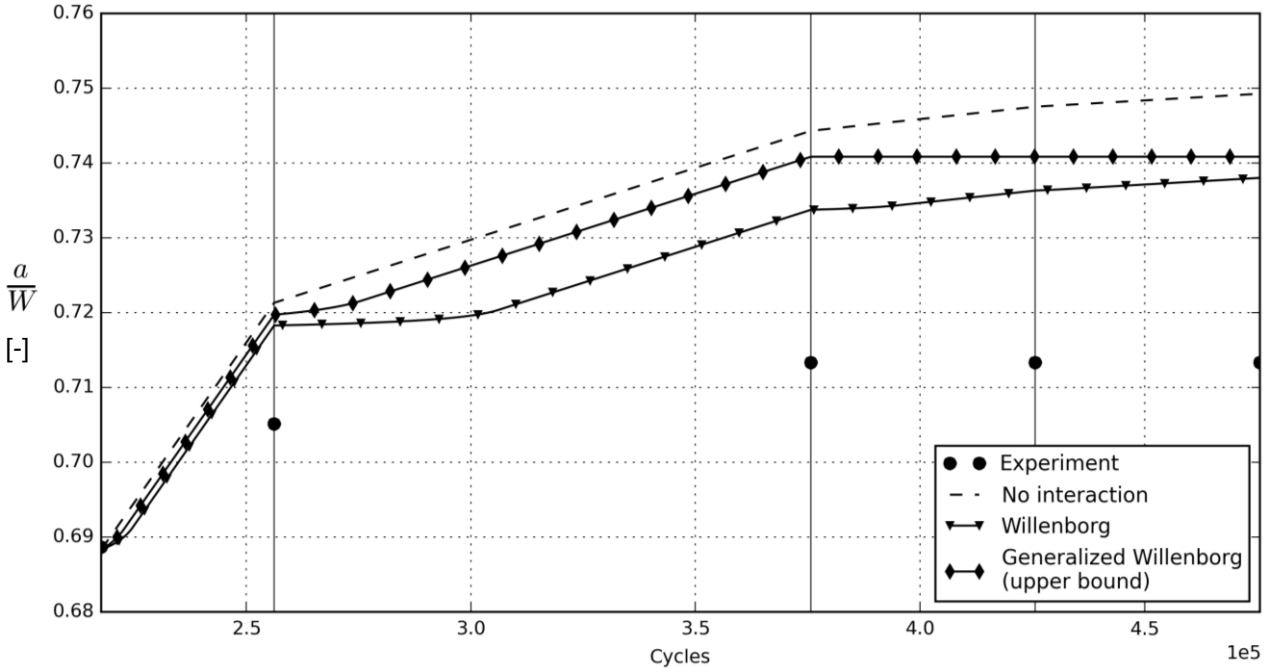

Figure 5: Comparison of the Willenborg and Generalized Willenborg model

employing the Paris law for crack growth rate calculations. It can be deduced from Eq. (6) that retardation is only quantified through the reduction of ΔK by $(K_{\mathrm{red}} - K_{\mathrm{min}})$. This way only part of the effect is captured. As $R_{\mathrm{eff}} < R$, incorporating the load ratio effect would improve predictions as crack growth rate would be lower and retardation would be higher. The Generalized Willenborg model underestimates the retardation effect even more, although crack arrest is correctly predicted. The most obvious cause is the shut-off overload ratio of the material, which takes values below 2. The proportionality factor λ thus generally decreases K_{red}, and therefore the amount of retardation, as is shown in Figure 6. An advantage of the proportionality factor is the correct prediction of crack arrest.

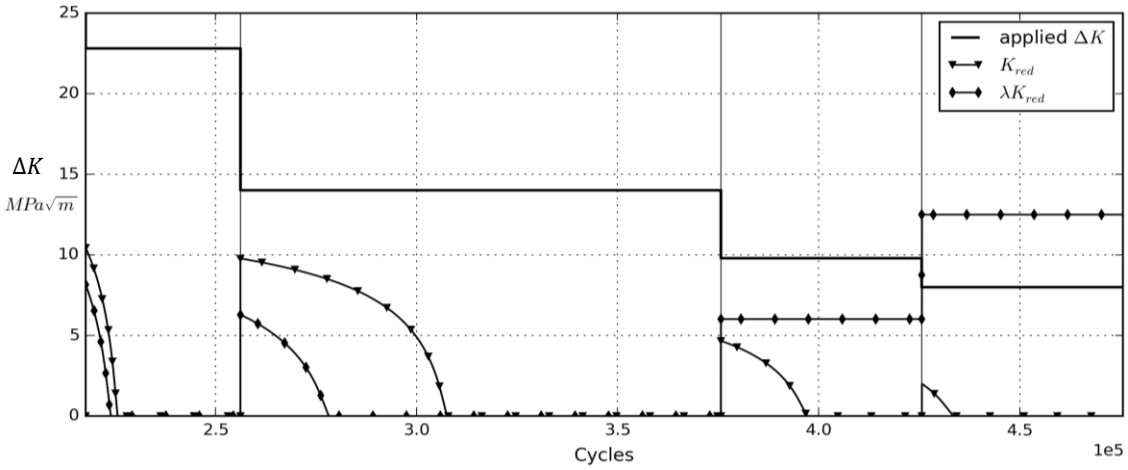

Figure 6: Influence of the proportionality factor λ on K_{red}

5 CONCLUSIONS

In this work, the capabilities of several crack tip plasticity models were compared regarding the prediction of retardation and crack arrest in variable amplitude fatigue. It is concluded that the Modified Wheeler model offers the most potential for applications in which only basic fatigue properties of the material are known. Consequently, the capabilities of the Willenborg model cannot be objectively assessed in this case, as at least one additional Paris curve is required, so that the load ratio effect can be estimated. Furthermore, all crack tip plasticity models would benefit from a more detailed determination of the shut-off load ratio as a function of applied SIF range.

6 REFERENCES

[1] O. E. Wheeler, “Spectrum Loading and Crack Growth,” *Journal of Basic Engineering*, vol. 94, no. 1, p. 181, 1972.

[2] J. Willenborg, R. M. Engle, and H. A. Wood, “A crack growth retardation model using an effective stress concept,” *Technical memorandum 71-1-FBR*. Wright-Patterson Air Force Base, Dayton, USA, 1971.

[3] J. P. Gallagher, “A generalized development of yield zone models,” *Technical memorandum FBR-74-28*. Wright-Patterson Air Force Base, Dayton, USA, 1974.

[4] J. P. Gallagher and T. F. Hughes, “Influence of yield strength on overload affected fatigue crack growth behavior in 4340 steel,” Dayton, USA, 1974.

[5] T. D. Gray and J. P. Gallagher, “Predicting Fatigue Crack Retardation Following a Single Overload Using a Modified Wheeler Model,” in *Mechanics of Crack Growth*, Philadelphia, USA: ASTM STP 590, 1976, pp. 331–344.

[6] R. C. Dragt, J. Maljaars, and J. T. Tuitman, “Including load sequence effects in the fatigue damage estimation of an offshore wind turbine sustructure,” in *Proceeding of International Ocean and Polar Engineering Conference*, 2016, pp. 199–205.

[7] S. De Tender, “Variable amplitude fatigue in offshore structures,” Master dissertation, Ghent University, 2016.

[8] S. De Tender, N. Micone, and W. De Waele, “Online fatigue crack growth monitoring with clip gauge and direct current potential drop,” *International Journal Sustainable Construction & Design*, vol. 7, no. 1, p. 6, 2016.

[9] T. L. Anderson, *Fracture Mechanics: Fundamentals and Applications*, 3rd ed. CRC Press, 2005.

[10] W. Guo, “Three-dimensional analyses of plastic constraint for through-thickness cracked bodies,” *Engineering Fracture Mechanics*, vol. 62, no. 4–5, pp. 383–407, 1999.

[11] H. J. C. Voorwald, M. A. S. Torres, and C. C. E. Pinto Júnior, “Modelling of fatigue crack growth following overloads,” *International Journal of Fatigue*, vol. 13, no. 5, pp. 423–427, 1991.

[12] H. Alawi, “Designing reliably for fatigue crack growth under random loading,” *Engineering Fracture Mechanics*, vol. 37, no. 1, pp. 75–85, 1990.

[13] B. C. Sheu, P. S. Song, and S. Hwang, “Shaping exponent in wheeler model under a single overload,” *Engineering Fracture Mechanics*, vol. 51, no. 1, pp. 135–143, 1995.

[14] T. D. Gray, “Fatigue crack retardation following a single overload,” *Technical memorandum AFFDL-TM-73-137-FBR*. Wright-Patterson Air Force Base, Dayton, USA, 1973.

[15] T. Machniewicz, “Fatigue crack growth prediction models for metallic materials,” *Fatigue & Fracture of Engineering Materials & Structures*, vol. 36, no. 4, pp. 293–307, 2013.

[16] N. Micone, W. De Waele, and S. Chhith, “Towards the understanding of variable amplitude fatigue,” *Mechanical Engineering Letters*, vol. 12, pp. 110–121, 2015.